A EUROPEAN JOURNAL OF CHEMICAL BIOLOGY

CHEMBIOCHEM

SYNTHETIC BIOLOGY & BIO-NANOTECHNOLOGY

Accepted Article

Title: Synthesis and Antineoplastic Applications of TPE Appended Organometallic Iridium(III) Complexes

Authors: Xicheng Liu, Xiangdong He, Xiaojing Zhang, Yongling Wang, Jiaying Liu, Xiujuan Hao, Yue Zhang, Xiang-Ai Yuan, Laijin Tian, and Zhe Liu

To be cited as: *ChemBioChem* 10.1002/cbic.201900268

Link to VoR: http://dx.doi.org/10.1002/cbic.201900268

A Journal of ChemPubSoc Europe

WILEY-VCH

www.chembiochem.org

WILEY-VCH

FULL PAPER

Synthesis and Antineoplastic Applications of TPE Appended Organometallic Iridium(III) Complexes

Xicheng Liu*[a], Xiangdong He[a], Xiaojing Zhang[a], Yongling Wang[a], Jiaying Liu[a], Xiujuan Hao[a], Yue Zhang[a], Xiang-Ai Yuan[a], Laijin Tian[a], Zhe Liu[a]*

Dedication ((optional))

Abstract: Iridium^{III} (Ir^{III}) complexes have attracted more and more attention because of their potential antineoplastic activity for the past few years. In this study, four Ir^{III} complexes of the type [(η^5-Cp^x)Ir(N^N)Cl]PF_6 (**1** and **2**) and [$Ir(Phpy)_2$(N^N)]PF_6 (**3** and **4**) have been synthesized and characterized. Complexes exhibit potential antineoplastic activity towards A549 cells, especially for complex **1** (IC_{50}: 3.56±0.5 μM), which was nearly six times of *cis*-platin (21.31±1.7 μM). Additionally, these complexes show some selectivity for cancer cells versus normal cells. Complexes could be transported by serum albumin (binding constant changed from 0.37~81.71×10^5 M^{-1}). Ir^{III} complexes (**1** and **2**) could catalyze the change of NADH to NAD^+ (TONs: 43.2, 11.9) and induce the accumulation of reactive oxygen species, which confirmed the antineoplastic mechanism of oxidation, while cyclometalated complexes (**3** and **4**) could target the lysosome (PCC: 0.73), lead to lysosomal damage and induce apoptosis. Understanding the mechanism of action would help further structure-activity optimization on these novel Ir^{III} complexes as emerging cancer therapeutics.

Introduction

The potential antineoplastic value of transition metal complexes has been widely recognized since the discovery of *cis*-platin (*cis*-diamminedichloridoplatinum(II)) by Rosenberg *etc.* in 1965.[1] Despite of numerous drawbacks, including strong resistance, poor selectivity, unclear mechanism of action, and serious adverse effects, platinum-based drugs are still considered as the most active chemotherapeutic agents and widely used.[2] In fact, treatment with platinum-based or platinum-related drugs accounts for over 50% of all chemotherapeutic regimens.[3] To solve these limitations, some alternative metals which showing different from *cis*-platin in antineoplastic mechanism and target sites have been developed and evaluated. In spite of the challenging, however, understanding the behavior of these complexes in tumor cells would still benefit for the design and improvement.[4]

Very recently, organometallic iridium^{III} (Ir^{III}) complexes have attracted much attention because of their potential anticancer activity towards various tumor cells.[5] Ir^{III} antitumor complexes can be classified as two main types: half-sandwich structure and cyclometalated structure complexes, and the general form can be expressed as [(Cp^x)Ir(L^L)Z]PF_6 and [$Ir(Phpy)_2$(L^L)]PF_6, respectively, where PF_6 is the common counter ion, Z is an chlorine anion or a neutral substituted pyridyl ligand, L^L is a chelating bidentate ligand (such as N^N, C^N and N^O *etc.*), and Cp^x and Phpy represents the electron-rich cyclopentadienyl group and 2-Phenylpyridine or its derivatives, respectively. Interestingly, the nature of all the parts around central iridium atom have a significant effect on the antineoplastic activity of these complexes, among these, the type and the position of the substituents on the L^L-chelating ligand were the most studied, and fine-regulating of which could effectively modulate the mechanism of uptake, target site of intracellular, and even the effects on the intracellular tissues.[6] Moreover, the prominent targeted fluorescence characteristics of organicmetallic Ir^{III} complexes provided the chance to investigate the microscopic mechanism of action. Studies showed that organicmetallic Ir^{III} complexes could enter cells in an energy-dependent or nonenergy-dependent mode, target lysosomes, mitochondria, endoplasmic reticulum or other cellular tissues, and lead to lysosomal damage, change of mitochondrial membrane potential or endoplasmic reticulum stress, and eventually induce apoptosis.[7]

As a typical aggregation-induced emitting (AIE) fluorescence group, tetraphenylethylene (TPE) has a propeller-shaped structure and the rotatable peripheral benzene rings, and now widely used in molecular design due to their distinctive luminescence property and easy modification.[8] Recently, many research achievements of TPE derivatives have been applied in the fields of organic light-emitting diode (OLED)[9], chemical sensing[10] and biological sensing[11]. However, the study of TPE applied to organometallic antineoplastic field was rare. It was established that the introduction of small molecular luminescent group to organometallic Ir^{III} complexes could effectively control antineoplastic activity and the target position in organelle.[12] Above all, in this study, four organometallic Ir^{III} complexes of the type [(Cp^x)Ir(N^N)Cl]PF_6 and [$Ir(Phpy)_2$(N^N)]PF_6 (**Figure 1**) have been synthesized and characterized. Activity of target complexes towards A549, BESA-2B and 16HBE cells was obtained by MTT (3-(4,5-Dimethylthiazol-2-yl)-2,5-diphenyl tetrazolium bromide) assay. Bovine serum albumin binding experiments were utilized to verify the transport mechanism of these complexes. Compared with cyclometalated Ir^{III} TPE complexes (**3** and **4**), half-sandwich

[a] *Institute of Anticancer Agents Development and Theranostic Application, The Key Laboratory of Life-Organic Analysis and Key Laboratory of Phar maceutical Intermediates and Analysis of Natural Medicine, School of Chemistry and Chemical Engineering, Qufu Normal University, Qufu 273165, China.*

Corresponding author (X. Liu) E-mail: chemlxc@163.com; Fax: 05374456301. (Z. Liu) E-mail: liuzheqd@163.com; Fax: 05374456301.

Supporting information for this article is given via a link at the end of the document.((Please delete this text if not appropriate))

Ir^{III} TPE complexes (**1** and **2**) could induce the production of reactive oxygen species, which confirmed the antitumor mechanism of oxidation. Due to the favorable targeted fluorescence property, complexes **3** and **4** could target the lysosome in *vivo*, lead to lysosomal damage, arrest the cell cycle, and eventually induce apoptosis. The results suggest that TPE-appended Ir^{III} complexes are of great significative for further evaluation as antineoplastic drugs.

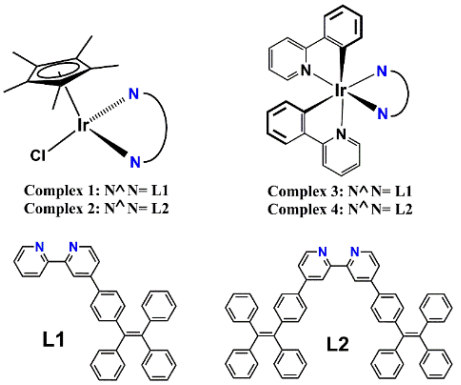

Figure 1. Structures of as-synthesized organometallic Ir^{III} TPE complexes.

Results and Discussion

Target Ir^{III} TPE complexes were synthesized by dimer and N^N-chelating ligands in good yields at ambient temperature,[13] and the N^N ligands were synthesized by Suzuki reaction between tetraphenylethylene boric acid and the corresponding bromopyridine compounds under N_2 (**Scheme 1**).[14] Multiple attempts to grow single crystals failed because of the "propeller-shaped" structure of TPE molecule leading to the major steric hindrance for target Ir^{III} complexes. Instead, the N^N-chelating ligands (L_1 and L_2) and target complexes (**1**-**4**) were characterized by nuclear magnetic resonance spectrum (NMR) and mass spectroscopy (MS), and all complexes were isolated as PF_6 salts. Deuterated reagent DMSO (2.50 ppm) and $CHCl_3$ (7.26 ppm) were used as the solvent for testing NMR of complexes. Hydrogens and carbons of the five methyl groups on Cp ring is shown in 1.66, 1.67 ppm and 8.58, 8.60 ppm for complex **1** and **2** in ^1H and ^{13}C NMR spectrum, and which on the benzene ring and pyridine are shown in the range of 6.20~9.15 ppm and 119.48~167.86 ppm, respectively. Target complexes were soluble in common organic solvents such as methanol, dimethyl sulfoxide and chloroform, insoluble in the ether, hexane and petroleum ether. Complexes **1** and **3**, a specially selected complexes, show the thermal decomposition temperatures (T_d) of 323.8 and 451.5 °C (**Figure S1**), respectively, which indicate that Ir^{III} TPE complexes possess good thermal stability. Aqueous stability of complexes **1** and **3** was also monitored in 50% CH_3OH/50% H_2O (*v/v*) by ultraviolet-visible (UV-vis) absorption spectrum at 298 K for 8 h, and no obvious changes for the absorbance were observed (**Figure S2**). The studies confirmed that TPE-appended Ir^{III} complexes possess sufficient stability for further biological assays.

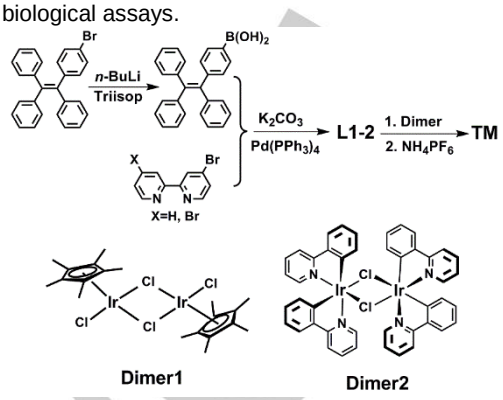

Scheme 1. Design strategy of of organometallic Ir^{III} TPE complexes.

1 Cytotoxicity test

The cytotoxicity of target complexes (**1**-**4**), TPE-unattached structural Ir^{III} complexes **5** ([(η^5-C_5Me_5)Ir(bipy)Cl]PF_6) and **6** ([Ir(Phpy)$_2$(bipy)]PF_6), *cis*-platin, Dimer (**1** and **2**) and chelating ligands (L_1 and L_2) were determined by the MTT (3-(4,5-Dimethylthiazol-2-yl)-2,5-diphenyl tetrazolium bromide) assay after 24 h treatment towards A549 lung cancer cells (the leading cause of death in both developed and developing countries). As shown in **Table 1**, compared with dimer, chelating ligands and TPE-unattached complexes, target Ir^{III} TPE complexes (**1**-**4**) exhibit potential antineoplastic activity, and the best of which (complex **1**) was nearly six times of *cis*-platin that widely used in the clinic. This conclusion proves that the introduction of TPE molecules is beneficial to enhance the antineoplastic activity of organometallic iridium complex.

Table 1 Inhibition of growth against A549, BESA-2B and 16HBE cells by complexes 1–6, *cis*-platin, dimer and chelating ligands after 24 h.

Complex	IC_{50} (μM)		
	A549	BEAS-2B	16HBE
1	3.56±0.5	6.31±0.9	6.61±0.2
2	17.27±0.1	20.52±1.4	35.10±0.7
3	32.73±0.5	40.38±0.3	21.04±0.5
4	>100	>100	>100
5	>100	/	/
6	40.33 ± 0.8	/	/
Cis-platin	21.31 ± 1.7	/	/
Dimer **1**	>100	/	/
Dimer **2**	>100	/	
L_1	>100	/	/
L_2	>100	/	/

Half-sandwich Ir^{III} complexes (**1** and **2**) exhibit better antineoplastic activity than cyclometalated structure complexes (**3** and **4**) under the same conditions. Studies show the antineoplastic activity of half-sandwich Ir^{III} complex mainly depends on the electronic properties of central iridium atom and the leaving group (Cl).[4d] To further understand how the ancillary ligands (TPE-appended bipyridine) influence the antineoplastic activity, the optimal configurations, the frontier molecular orbitals

and their electron cloud distribution were analyzed by density functional theory (DFT) calculation at the B3LYP/6-31G(d) (C, H, N, Cl)/lanl2dz (Ir) level.[15] As shown in **Figure 2**, the HOMOs of complexes **1** and **2** are mainly localized on the bipyridine ligand and the terminal TPE groups, while the LUMOs are mainly localized on the central iridium atom, bipyridine ligand, phenyl of TPE molecule connected with bipyridine and chlorine atom (the leaving group), which indicate that the introduction of TPE molecule improves the conjugate area and electron donor capacity of bipyridine chelating ligand,[16] thus increasing the electron cloud density of central iridium atoms, facilitating the break of Ir-Cl bonds and leading to the favorable antineoplastic activity. However, major dihedral angles between **P1** (pyridine ring) and **P2** (benzene ring of TPE molecule) ring are 29.63° and 29.93° for complexes **1** and **2**, respectively, which confirm that this improvement is limited. This conclusion could further be confirmed by the data of natural population analysis (NPA) and Wiberg bond order of Ir-Cl bond at the B3LYP/6-31G(d, p) (C, H, N, Cl)/SDD (Ir) level. The results of NPA charge population (**Table S1**) for Ir and Cl in complexes **1** and **2** were almost the same with the values of 0.19 and -0.33, respectively.[17] Ir-Cl bond levels were also shown almost the same values for complex **1** (0.7553) and **2** (0.7539). This conclusion is consistent with the hypothesis of optimal configuration that the conjugation of chelating ligands is finite because of the major dihedral angles between bipydine and TPE molecule, which leads to the limited improvement of electron cloud density for the central iridium atom, so there's not much difference in Ir-Cl bond levels of complexes **1** and **2**.

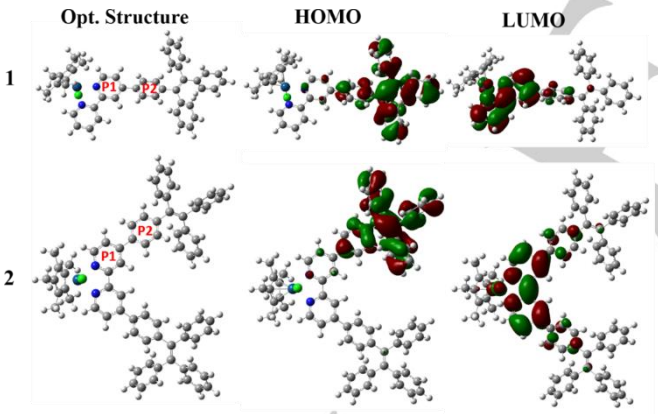

Figure 2. Calculated optimal configurations, HOMO and LUMO diagrams of complexes **1** and **2**.

The partition coefficients (*logP*) of **complexes 1-4** in oil/water were determined by inductively coupled plasma mass spectrometry and the values were -0.33, 0.12, 1.05 and 1.44, respectively. These results indicate that the introduction of too many TPE groups enhances the lipid solubility of the complexes, but at the same time weakens their water solubility, thus affecting the antineoplastic activity of complexes.[6d,7a] Studies have also confirmed that the lipid solubility and water solubility of the complexes can be improved, and the antineoplastic activity of complexes can be effectively adjusted by reasonable design for the type and number of ligands.[18]

In addition, the cytotoxicities of complexes **1-4** to human bronchial epithelial cells (16HBE) and lung epithelial cells (BEAS-2B) were further evaluated. As shown in **Table 1**, these complexes show some selectivity for cancer cells versus normal cells, especially for complexes **1** and **2**, but it is not obvious. Therefore, more structural modifcation is necessary to improve the selectivity in future work.

2 Reaction with NADH

Being cofactor, NADH (the reduced state of nicotinamide adenine dinucleotide) plays a major role in numerous biological process such as cell death, antioxidation, oxidative stress and energy metabolism.[19] In *vivo*, the transformation from NADH to NAD^+ could induce the accumulation of reactive oxygen species (ROS) H_2O_2 and lead to apoptosis, which provided an antineoplastic mechanism of oxidation.[20] As shown in **Figures 3a** and **S3**, there are significantly decreased absorbance at 339 nm (the maximum UV-vis absorbance of NADH) and increased that at 259 nm (the maximum absorbance of NAD^+) with the addition of half-sandwich Ir^{III} complexes (**1** and **2**), especially for complex **1.**[21] However, almost no changes occur for cycloiridium complex (**3** and **4**). The turnover numbers (TONs) of complexes **1** (43.2), **2** (11.9) **3** (3.0) **4** (2.6) were calculated by measuring the difference at 339 nm (**Figure 3b**), which was consistent with the result that half-sandwich Ir^{III} complexes possessed better antineoplastic activity than cyclometalated Ir^{III} complexes.

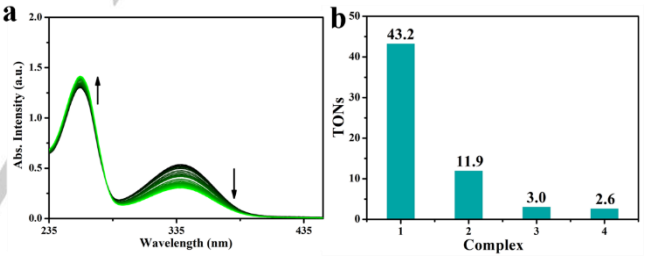

Fig. 3 (a) UV-vis spectrum of NADH (100 μM) dealed with complex **1** (1 μM) in 10% MeOH/90% H_2O (*v/v*) at 298 K for 8 h; (b) The TONs of complexes.

3 Study of BSA interactions

Being the most abundant protein in plasma, serum albumin (SA) plays an major role in drug transport and metabolism, and then the research on the interactions of target complexes and SA is beneficial to investigate the transport mechanism of drugs. [22] Because of the similar structure, easy availability and low price, bovine serum albumin (BSA) could be a cost-efficent alternative to human serum albumin (HSA).[23] Therefore, in this study, BSA was used to determine the interaction between target complexes and protein. As shown in **Figures 4a** and **S4**, with the increase of Ir^{III} TPE complexes, the maximum absorption of 218 nm (the absorption of BSA) decreased, which indicated Ir^{III} TPE complexes could act on BSA and induce alphahelical interference. Meanwhile, due to the influence of polar solvent (water), a significant red shift was found at 218 nm.[24] Additionally, the

absorption peaks increased gradually at 278 nm, which demonstrated that Ir^{III} TPE complexes might interact with Tryptophan, Tyrosine or Phenylalanine (three aromatic acid residues in BSA) in the microenvironment.[25]

Binding properties between Ir^{III} TPE complexes and BSA could also be determined by fluorescence spectra (**Figures 4b** and **S5**), and which were calibrated to correct the "inner filter" effect.[26] With the increase of target complex, there is a significantly decrease at 343 nm (the flurescene emission peak of BSA) at 298 K. The quenching rate constant (K_q) and Stern–Volmer quenching constant (K_{sv}) were calculated using the classical Stern-Volmer equation (**Figure S6**), and the binding constant (K_b) and binding site number (n) of complexes were calculated by the Scatchard equation (**Figure S7**).[27] As shown in **Table 2**, the K_q of all complexes ranged from 0.68×10^{13} to 2.88×10^{13} M^{-1} s^{-1}, which were almost three orders of magnitude higher than that of a pure dynamic quenching mechanism (2.0×10^{10} M^{-1} s^{-1}).[28] This conclusion indicate that static quenching mechanism plays a decisive role in the process of Ir^{III} TPE complexes acting on BSA. In addition, the n and the K_b of complex **1** are the best among these Ir^{III} complexes, which indicate that the introduction of too many TPE molecules will increase the steric hindrance between the target complex and BSA. And also, this conclusion is consistent with the result of cytotoxicity test that complex **1** show the best antineoplastic activity than the other complexes.

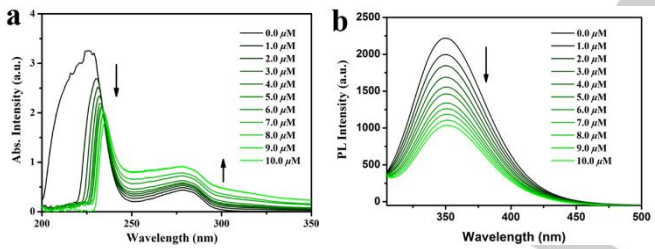

Figure 4. (a) UV-vis spectrum of BSA (10.0 μM) in 5 mM Tris-HCl/50 mM NaCl buffer solution (pH: 7.2) with the increase of complexe **2** (0-10.0 μM). (b) Fluorescence spectra of BSA (10.0 μM; λ_{ex} =280 nm; λ_{em} =343 nm) in the absence and presence of complex **2** (0-10.0 μM).

Table 2. The values of Ksv, Kb and Kq for as-synthesized IrIII complexes.

Complex	K_q (10^{13} $M^{-1}S^{-1}$)	K_{sv} (10^5 M^{-1})	K_b (10^5 M^{-1})	n
1	2.88	2.88±0.16	81.71	1.27
2	1.11	1.11±0.15	3.86	1.09
3	1.08	1.08±0.15	1.40	1.02
4	0.68	0.68±0.18	0.37	0.94

4 Apoptosis Assay

In order to clarify whether Ir^{III} TPE complex could induce apoptosis, A549 cells were treated with selected complexes **1** and **3** at the concentration of 0.5, 1.0, 2.0 and 3.0 × IC_{50}. After staining with Annexin V/Propidium Iodide, the data were obtained by flow cytometry.[29] As shown in **Figure 5** and **Tables S2-S3**, complexes induce a dose-dependent increase in the percentage of apoptotic cells after 24 h of treatment. The percentage of early apoptosis and late apoptosis cells increased from 1.7% and 9.8% to 8.1% and 65.9% when the concentration changed from 0.5 × IC_{50} to 3.0 × IC_{50} for complex **1**. In addition, about 43.5% of A549 cells treated with complex **3** were undergoing apoptosis, 41.9% of which were in late apoptosis. In comparison, 95.1% of A549 cells survived for the control under the same conditions. This conclusion was consistent with the results of the MTT assay, and further confirmed Ir^{III} TPE complexes could lead to functional decline of tumor cells and induce apoptosis.

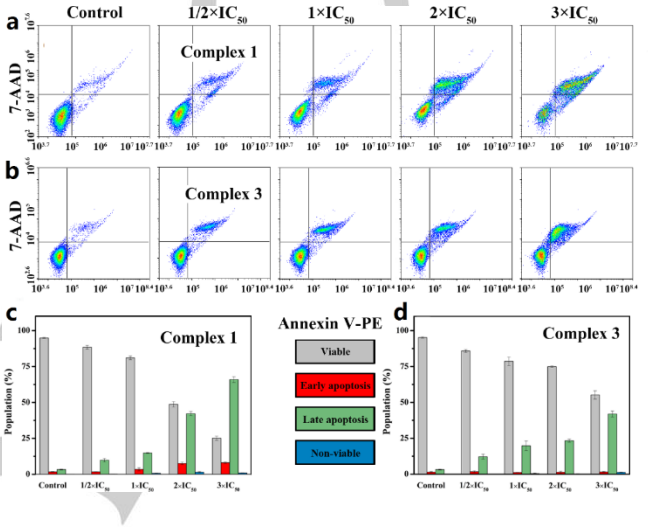

Figure 5. Apoptosis analysis of A549 cells after 24 h of exposure to complex **1** (a) and **3** (b) were determined by flow cytometry; Histogram of apoptosis analysis after treated with complexes **1** (c) and **3** (d). Data are quoted as mean ± SD of three replicates.

5 Cell Cycle Analysis

The cell cycle was monitored by flow cytometry to determine whether cell function decline was caused by the antiproliferative activity of Ir^{III} TPE complexes.[30] As shown in **Figure 6** and **Tables S4-S5**, A549 cells were exposed to complexes **1** and **3** at the concentrations of 0.25, 0.5 and 1.0 × IC_{50} for 24 h. The percentages of cells in the Sub-G1 phase increased from 61.3% to 72.5% for complex **1** at the concentration of 1.0 × IC_{50}. While for complex **3**, the Sub-G1 phase increased by only 1.6%. These results confirm that Ir^{III} TPE complexes could disturb the cell cycle mainly in the Sub-G1 phase and eventually induce apoptosis, especially for half-sandwiched Ir^{III} complexes (**1** and **2**).

6 Induction of ROS

Reactive oxygen species (ROS) is a single electron reduction product of a class of oxygen, and the accumulation in *vivo* will lead to intrinsic apoptosis, which is used to explore the function mechanism of anticancer agents.[4d] To further evaluate the catalytic characteristic of Ir^{III} TPE complexes, the levels of ROS were determined by flow cytometry after exposure to complexes **1**-**4** for 24 h at the concentrations of 0.25 × IC_{50} and 0.5 × IC_{50}. As shown in **Figure 7**, compared with the positive and negative, 82.01% and 89.08% of A549 cells were at high ROS levels for complexes **1** and **2**, respectively. This significant

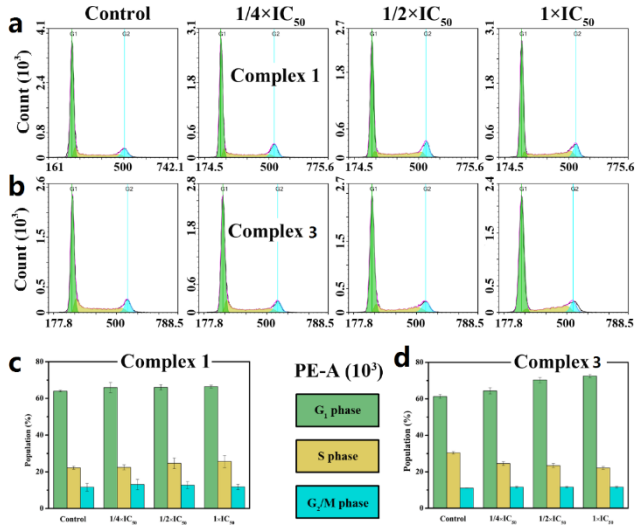

Figure 6. Cell cycle analysis of A549 cells after 24 h of exposure to complexes **1** (a) and **3** (b) by flow cytometry. The histogram of cell cycle distribution of A549 cells for control and complexes **1** (c) and **3** (d). Data are quoted as mean ± SD of three replicates.

improvement of ROS level provides an effective basis for the apoptosis of A549 cells, and further confirmed the antineoplastic mechanism of oxidation for half-sandwich Ir^{III} TPE complexes (**1** and **2**). However, for cyclometalated Ir^{III} TPE complexes (**3** and **4**), almost no A549 cells are in ROS level, which is consistent with the result of NADH test, and also indicate that cyclometalated Ir^{III} TPE complexes possess different antineoplastic mechanism compared with half-sandwiched Ir^{III} TPE complexes.

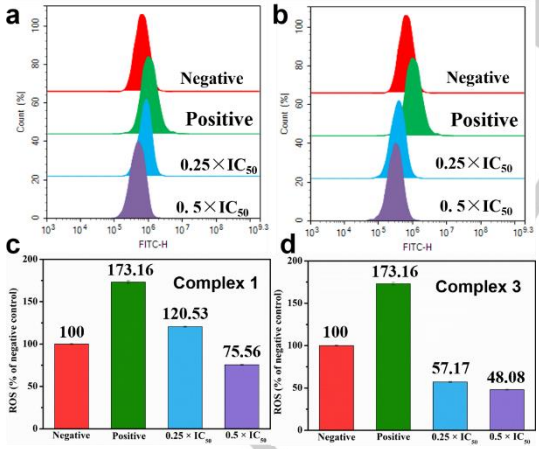

Figure 7. Effect of complexes **1** (a, c) and **3** (b, d) on intracellular ROS levels in A549 lung cancer cells treated at the indicated concentrations for 24 h.

7 Evaluation of antineoplastic mechanism for cyclometalated Ir^{III} TPE complexes

As the most popular luminous materials, cyclometalated Ir^{III} complexes have been widely used in the field of organic light-emitting diodes (OLEDs) not only because of the short excited state lifetime, but also the high thermostability and easily adjustable emission color.[31] Photophysical properties of complexes **3** and **4** were determined by UV-vis and photoluminescence (PL) spectrum. As shown in **Figure 8**, complexes **3** and **4** show almost the same photophysical properties, which have a strong intraligand absorption band (π-π*) at around 250-300 nm (ε >14000 M^{-1} cm^{-1}) and a weaker metal-to-ligand charge-transfer (MLCT) transition band at around 350-450 nm and exhibit a yellow intense emission located at ~572 nm. Electron cloud distribution of the frontier molecular orbitals (**Figure S8**) shows that the HOMOs of **3** and **4** are mainly localized on TPE molecules, and the LUMOs are mainly localized on the Ir atom and dipyridine ligand. In addition, the distribution of HOMO doesn't increase with the addition of TPE molecules for complex **4**. This conclusion indicates that TPE-appended ancillary ligands have little effect on their electronic structures, and then, which is in agreement with the result that complex **3** possess almost the same UV-vis and PL spectrum with **4**.

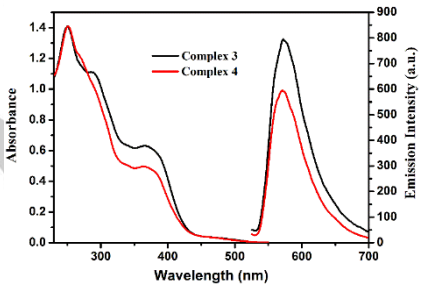

Figure 8. UV-vis and PL of complexes **3** and **4** in methanol solution (1.0×10^{-5} M).

Due to favorable luminescence property for cyclometalated Ir^{III} TPE complexes, laser confocal microscopy was used to determine the subcellular localization in A549 cells. Lyso Tracker Red DND-99 (LTRD) and Mito Tracker Deep Red (MTDR) were utilized as lysosomes and mitochondria fluorescence probes, respectively.[7b,32] As shown in **Figure 9**, complex **3** could effectively accumulate in lysosomes with the Pearson's co-localization coefficient (PCC) of 0.73 when incubated for 6 h. However, the PCC of mitochondrion-targeted for complex **3** is 0.12. The results indicate that cyclometalated Ir^{III} TPE complexes could effectively target lysosomes in *vivo*. Additionally, target complex did not cause abnormal cell death immediately, which made it easy to track changes in lysosomal morphology timely.

Lysosomes are acidic intracellular organelles and play an important role in many cellular processes, including post-translational protein maturation, receptor degradation, apoptosis, autophagy and the extracellular release of active enzymes. As the organelles, lysosomes could break down proteins, nucleic acids, polysaccharides and other biological macromolecules. When damaged, they release hydrolases that digest the entire cell, and

eventually promote apoptosis.[33] Acridine orange (AO), an effective probe to determine the integrity of the acidic organelles (which emitting red fluorescence in lysosomes and green fluorescence in the cytosol and nuclei), was used as the probe to study the lysosomal integrity of A549 cells. A549 cells were incubated with complex **3** (10 μM) for 2 h and 6 h, and then stained with AO (5 μM). As shown in **Figure 10**, there was a significant decrease in red fluorescence when cells hatched in complex **3** (1.0 × IC_{50}) for 2 h, and obvious lysosomal damage was found after 6 h. The results confirmed that cyclometalated Ir^{III} TPE complexes could target lysosome, lead to lysosomal damage, and eventually induce apoptosis.

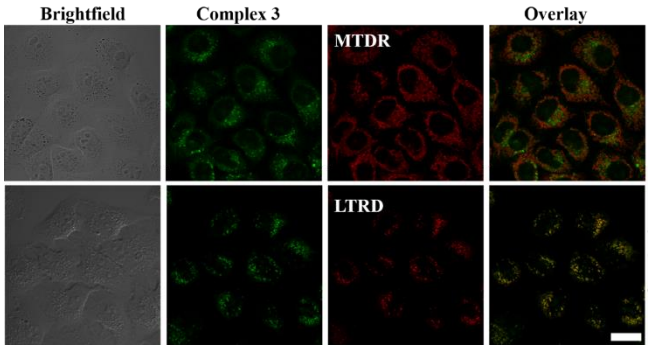

Figure 9. Determination of intercellular localization for complex **3**. A549 cells were stained with LTRD and MTDR (200 nM) for 20 min and then incubated with complexes **3** (the concentration is equivalent to IC_{50}) for 6 h at 310 K. The complexes were excited at 488 nm and the emission was collected at 493-630 nm. LTRD was excited at 594 nm and the emission was collected at 549-651 nm. MTDR was excited at 644 nm and the emission was collected at 660- 720 nm. Scale bar: 20 μm.

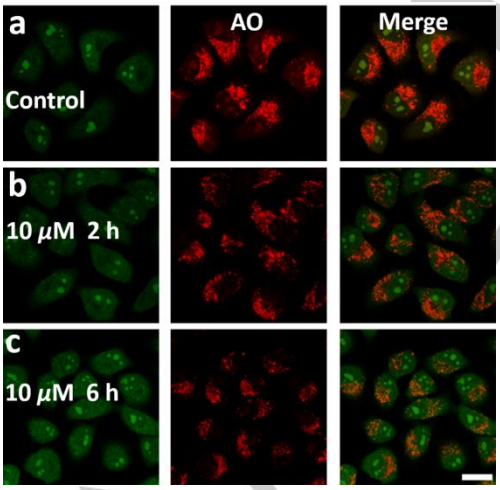

Fig. 10 (a) A549 cells were incubated with control (a) and complex **3** (10 μM) for 2 h (b) and 6 h (c) and then stained with AO (5 μM). λ_{ex} = 488 nm, λ_{em} = 510 ± 30 nm (green) and 625 ± 30 nm (red). Scale bar: 20 μm.

Conclusions

In this paper, four organometallic $iridium^{III}$ complexes were synthesized with simple synthetic procedures. The introduction of TPE molecules could effectively adjust the lipid solubility of complex drugs, and endowed Ir^{III} complexes with potential antineoplastic activity, the best of which (complex **1)** was nearly six times of *cis*-platin under the same conditions. Additionally, these complexes show some selectivity for cancer cells versus normal cells**.** Complexes could be transported through serum albumin, disturbed the cell growth cycle and induced apoptosis. Among these, half-sandwiched Ir^{III} complexes (**1** and **2**) could effectively catalyze the conversion of NADH to NAD^+ and induce the accumulation of ROS, which present the antitumor mechanism of oxidation. Additionally, $cycloiridium^{III}$ complexes could specifically accumulate in lysosomes, lead to the lysosomal damage, and eventually induce apoptosis. Above all, TPE-appended $iridium^{III}$ complexes could be a promising candidate for further evaluation as antineoplastic drugs.

Experimental Section

Materials

Iridium trichloride, 1,2,3,4,5-pentamethyl-cyclopentadiene(95%), 4,4'-dibromo- 2,2'-bipyridine, 4-bromo-2,2'-bipyridine, tetratriphenylphosphine palladium, anhydrous potassium carbonate, diphenylmethane, 4-bromodiphenylketone, *n*-butyllithium, *p*-toluene sulphonic acid, triisopropyl borate and phenylpyridine were purchased from Rhea biotechnology co. LTD. For the biological experiments, DMEM medium, fetal bovine serum, penicillin/streptomycin mixture and trypsin/EDTA were purchased from Sangon Biotech. A549 lung cancer cells were obtained from Shanghai Institute of Biochemistry and Cell Biology (SIBCB).

Syntheses and characterization

*Synthesis of 4-(4-(1,2,2-triphenylvinyl)phenyl)-2,2'-bipyridine (**L_1**):*

Tetraphenylboric acid (0.56 g, 1.5 mmol), 4-bromo-2,2'-bipyridine (0.24 g, 1.0 mmol), tetratriphenylphosphine palladium (0.12 g, 0.1 mmol), anhydrous potassium carbonate (0.42 g, 3.0 mmol) were added into a 150 mL round-bottom flask under nitrogen. 60 mL toluene and 15 mL water were deoxygenated and added, then the reaction mixture was refluxed for 30 h (monitored by thin-layer chromatography) and extracted with dichloromethane. The organic layer was dried over anhydrous magnesium sulfate. After solvent evaporation, the crude product was purified by silica gel column chromatography (Petroleum ether: ethyl acetate =50:1 as eluent) to give purified product (**L_1**). Yield 0.27 g (55.4%). ^{1}H NMR (500 MHz, $CDCl_3$) δ 8.63 (t, *J* = 5.3 Hz, 2H), 8.58 (s, 1H), 8.41 (s, 1H), 7.78 (d, *J* = 7.5 Hz, 1H), 7.47 (d, *J* = 8.2 Hz, 3H), 7.27 (s, 1H), 7.13 – 7.02 (m, 11H), 7.02 – 6.93 (m, 6H).

L_2 was synthesized by tetraphenylboric acid and 4,4'-dibromo-2,2'-bipyridine using the same method as **L_1**. Yield 51.2%. ^{1}H NMR (500 MHz, $CDCl_3$) δ 9.14 (s, 2H), 8.81 (d, *J* = 5.6 Hz, 2H), 7.80 (s, 2H), 7.74 (d, *J* = 8.1 Hz, 4H), 7.24 (s, 4H), 7.17 – 7.10 (m, 18H), 7.10 – 7.00 (m, 12H).

*Synthesis of target complexes **1**-**4***

Dimer (1 *equiv*) and chelating ligands (2 *equiv*) were stirred at ambient temperature overnight in methanol solution. Then hexafluorophosphate (8 *equiv*) were added to above solution and reacted for 4 h. Most of the solvent is concentrated in vacuum and kept at -20 °C for 12 h, filtered and washed with cold methanol and diethyl ether. The ^{1}H NMR and MADLI-TOF MS of complexes **1**-**4** are shown in **Figures S9** and **S10**. The concrete data are as follows:

$[(\eta^5\text{-}C_5Me_5)Ir(L_1)Cl]PF_6$ **(1)**: Yield 65.8%. ^{1}H NMR (500 MHz, DMSO): δ 9.06 – 8.97 (m, 3H, H-Py), 8.91 (d, *J* = 6.1 Hz, 1H, H-Py), 8.35 (t, *J* = 7.2 Hz, 1H, H-Py), 8.08 (dd, *J* = 6.1, 1.9 Hz, 1H, H-Py), 7.92 (d, *J* = 8.5 Hz, 1H, H-Py), 7.90 – 7.83 (m, 2H, H-TPE), 7.28 – 7.10 (m, 11H, H-TPE), 7.11

– 6.97 (m, 6H, H-TPE), 1.66 (s, 15H, H-CH_3). ^{13}C NMR (126 MHz, DMSO) δ 155.91, 155.42, 152.54, 152.36, 150.32, 146.65, 143.35, 143.33, 143.22, 142.39, 142.34, 140.68, 140.06, 132.83, 132.17, 131.18, 131.16, 131.08, 129.45, 128.50, 128.35, 127.59, 127.43, 127.30, 125.81, 125.74, 124.99, 121.32, 89.58 (C- Cp^x), 8.60 (CH_3-Cp^x); ESI-MS (*m/z*): Calcd for $C_{43}H_{44}ClIrN_3$ 830.513 $[M\text{-}PF_6]^+$; Found: 830.863. Calcd for $C_{43}H_{44}IrN_3$ 795.063 $[M\text{-}PF_6\text{-}Cl]^{2+}$; Found: 794.926.

$[(\eta^5\text{-}C_5Me_5)Ir(L_2)Cl]PF_6$ **(2)**: Yield 60.2%. ^{1}H NMR (500 MHz, DMSO): δ 9.15 (s, 2H, H-Py), 9.05 – 8.76 (m, 4H, H-Py), 8.08 (s, 2H, H-TPE), 7.93 (d, *J* = 7.6 Hz, 4H, H-TPE), 7.39 – 6.89 (m, 32H, H-TPE), 1.67 (s, 15H, H-CH_3). ^{13}C NMR (126 MHz, DMSO) δ 155.53, 151.83, 150.89, 147.00, 143.24, 143.19, 143.15, 143.12, 143.07, 142.61, 142.52, 139.65, 132.90, 132.54, 131.32, 131.27, 127.98, 127.91, 127.71, 126.95, 126.91, 126.80, 126.04, 89.46 (C-Cp^x), 8.55(CH_3-Cp^x); ESI-MS (*m/z*): Calcd for $C_{48}H_{46}ClIrN_3$ 892.584 $[M\text{-}PF_6]^+$; Found: 892.884. Calcd for $C_{48}H_{46}IrN_3$ 857.134 $[M\text{-}PF_6\text{-}Cl]^{2+}$; Found: 856.909.

$[Ir(Phpy)_2(L_1)]PF_6$ **(3)**: Yield 63.2%. ^{1}H NMR (500 MHz, DMSO) δ 9.15 (d, *J* = 8.2 Hz, 1H, H-Ar), 9.08 (s, 1H, H-Ar), 8.32 – 8.25 (m, 3H, H-Ar), 7.98 (dd, *J* = 5.9, 1.6 Hz, 1H, H-Ar), 7.96 – 7.85 (m, 7H, H-Ar), 7.80 (d, *J* = 5.9 Hz, 1H, H-Ar), 7.69 (dd, *J* = 11.7, 6.0 Hz, 2H, H-Ar), 7.63 (d, *J* = 5.4 Hz, 1H, H-Ar), 7.15 (ddd, *J* = 11.6, 10.5, 6.1 Hz, 12H, H-Ar/TPE), 7.06 – 6.98 (m, 8H, H-TPE), 6.91 (t, *J* = 7.4 Hz, 2H, H-TPE), 6.20 (dd, *J* = 7.1, 4.2 Hz, 3H, H-TPE). ^{13}C NMR (126 MHz, DMSO) δ 167.86, 167.61, 156.24, 155.59, 151.10, 150.59, 150.25, 150.23, 150.12, 148.88, 148.80, 148.59, 146.85, 143.59, 143.47, 143.37, 143.32, 143.24, 143.09, 142.42, 139.96, 139.82, 138.12, 133.04, 132.58, 131.82, 131.74, 131.33, 131.28, 130.87, 130.74, 128.21, 127.97, 127.91, 127.87, 127.71, 126.85, 126.75, 126.71, 125.47, 125.05, 124.81, 124.72, 123.59, 123.32, 122.65, 122.61, 122.11, 119.64, 119.51; ESI-MS (*m/z*): Calcd for $C_{54}H_{50}ClIrN_3$ 968.682 $[M\text{-}PF_6]^+$; Found: 967.818.

$[Ir(Phpy)_2(L_2)]PF_6$ **(4)**: Yield 66.5%. ^{1}H NMR (500 MHz, $CDCl_3$): δ 8.59 (s, 2H, H-Ar), 7.89 (d, *J* = 6.9 Hz, 4H, H-Ar), 7.77 – 7.65 (m, 6H, H-Ar), 7.60 – 7.45 (m, 6H, H-Ar), 7.20 (s, 4H, H-Ar), 7.16 – 6.97 (m, 34H, H-TPE), 6.92 (t, *J* = 7.2 Hz, 2H, H-TPE), 6.32 (d, *J* = 7.4 Hz, 2H, H-TPE). ^{13}C NMR (126 MHz, DMSO) δ 167.57, 156.08, 151.08, 150.60, 150.21, 149.00, 146.57, 143.61, 143.35, 143.29, 143.18, 142.26, 139.87, 138.12, 133.54, 132.49, 131.82, 131.38, 131.34, 131.30, 130.74, 127.93, 127.87, 127.71, 126.88, 126.83, 126.74, 126.71, 125.50, 124.68, 123.64, 122.55, 122.30, 119.48; ESI-MS (*m/z*): Calcd for $C_{48}H_{46}ClIrN_3O_2$ 1317.445 $[M\text{-}PF_6]^+$; Found: 1317.4.

Acknowledgements

We thank the University Research Development Program of Shandong Province (J18KA082) the Student's Platform for Innovation and Entrepreneurship Training Program (2018A043),, the National Natural Science Foundation of China (21671118 and 21703118), the Taishan Scholars Program, Shandong Provincial Natural Science Foundation (ZR2017MB038) and High Performance Computing Center of Qufu Normal University for support.

Keywords: Organometallic • Iridium complex • Tetraphenylethylene • Anticancer

[1] B. Rosenberg, L. V. Camp, T. Krigas, *Nature* **1965**, *205*, 698–699.

[2] L. Kelland, *Nat. Rev. Cancer* **2007**, *7*, 573–584.

[3] a) P. Gong, S. Ji, J. Wang, D. Dai, F. Wang, M. Tian, L. Zhang, F. Guo, Z. Liu, *Chem. Eng. J.* **2018**, *348*, 438–446; b) P. Zhang, P. J. Sadler, J. *Organomet. Chem.* **2017**, *839*, 5–14; c) J. Cao, C. Tan, M. Chen, N. Wu, D. Yao, X. Liu, L. Ji, Z. Mao, *Chem. Sci.* **2017**, *8*, 631–640.

[4] a) G. Li, R. Guan, L. Ji, H. Chao, *Coord. Chem. Rev.* **2014**, *281*, 100–113; b) C. G. Hartinger, N. Metzler-Nolte, P. J. Dyson, *Organometallics* **2012**, *31*, 5677–5685; c) J. J. Li, X. C. Liu, H. F. Zhang, X. X. Ge, Y. H. Tang, Z. S. Xu, L. J. Tian, X. A. Yuan, X. D. Mao, Z. Liu, *Inorg. Chem.* **2019**, *58*, 1710–1718; d) N. Muhammad, Z. J.Guo, *Curr. Opin. Chem. Biol.* **2014**, *19*, 144–153; e) X. C. Liu, Y. H. Tang, X D. He, X. X. Ge, J. Liu, X. Y. Meng, M. X. Shao, Y. M. Jin, L. J. Tian, Z. Liu, *J. Inorg. Biochem.* **2019**, *191*, 194–202.

[5] Z. Liu, P. J.Sadler, *Acc. Chem. Res.* **2014**, *47*, 1174−1185.

[6] a) H. R. Zhang, L. H. Guo, Z. Z. Tian, M. Tian, S. M. Zhang, Z. S. Xu, P. W. Gong, Z. X. Zheng, J. Zhao, Z. Liu, *Chem. Commun.* **2018**, *54*, 4421–4424; b) Z. S. Xu, D. L. Kong, X. D. He, L. H. Guo, X. X. Ge, X. C. Liu, H. R. Zhang, J. J. Li, Y. L. Yang, Z. Liu, *Inorg. Chem. Front.* **2018**, **5**, 2100–2105; c) X. D. He, M. Tian, X. C. Liu, Y. H. Tang, C. F. Shao, P. W. Gong, J. F. Liu, S. M. Zhang, L. H. Guo, Z. Liu, *Chem. Asian J.* **2018**, *13*, 1500–1509.

[7] a) X. D. He, X. C. Liu, Y. H. Tang, J. Y. Du, M. Tian, Z. S. Xu, X. Y. Liu, Z. Liu, *Dyes Pigments* **2019**, *160*, 217–226; b) L. He, Y. Li, C.-P. Tan, R. R. Ye, M. H. Chen, J. J. Cao, L.-N. Ji, Z. W. Mao, *Chem. Sci.* **2015**, *6*, 5409–5418; c) M. Ouyang, L. Zeng, H. Huang., C. Jin, J. Liu, Y. Chen, L.-N. Ji, H. Chao, *Dalton. Trans.* **2017**, *46*, 6734–6744; d) R. Cao, J. Jia, X. Ma, M. Zhou, H. Fei, *J. Med. Chem.* **2013**, *56*, 3636–3644; e) Y. L. Han, Z. Z. Tian, S. M. Zhang, X. C. Liu, J. J. Li, Y. R. Li, Y. Liu, M. Cao, Z. Liu, *J. Inorg. Biochem.* **2018**, *189*, 163–171.

[8] J. Mei, Y. Hong, J. W. Y. Lam, A. Qin, Y. Tang, B. Z. Tang, *Adv. Mater.* **2014**, *26*, 5429-5479; b) R. Hu, L. C. L. Nelson, B. Z. Tang, *Chem. Soc. Rev.* **2014**, *43*, 4494–4562.

[9] W. Yuan, P. Lu, S. Chen, J. W. Y. Lam, Z. Wang, Y. Liu, H. S. kwok, Y. Ma, B. Z. Tang, *Adv. Mater.* **2010**, **22**, 2159–2163.

[10] a) Y. Yu, A. J. Qin, C. Feng, P. Lu, K. M. Ng, K. Q. Luo, B. Z. Tang, *Analyst* **2012**, *137*, 5592–5596; b) Y. Yu, J. Liu, Z. Zhao, K. M. Ng, K. Q. Luo, B. Z. Tang, *Chem. Commun.* **2012**, *48*, 6360–6362.

[11] a) S. J. Chen, Y. N. Hong, Y. Liu, J. Liu, C. W. Leung, M. Li. R. T. K. Kowk, E. Zhao, J. W. Y. Lam, Y. Yu, B. Z. Tang, *J. Am. Chem. Soc.* **2013**, *135*, 4926–4929; b) C. W. T. Leung, Y. N. Hong, S. J. Chen, E. Zhao, J. W. Y. Lam, B. Z. Tang, *J. Am. Chem. Soc.* 2013, 135, 62–65; c) N. Zhao, M. Li, Y. L. Yan, J. W. Lam, Y. L. Zhang, Y. S. Zhao K. S. Wong, B. Z. Tang, *J. Mater. Chem. C* **2013**, *1*, 4640–4646.

[12] a) W. L. Ma, Z. Z. Tian, S. M. Zhang, X. D. He, J. J. Li, X. R. Xia, X. B. Chen, Z. Liu, *Inorg. Chem. Front.* **2018**, *5*, 2587–2597; b) F. Xue, Y. Lu, Z. Zhou, M. Shi, Y. Yan, H .Yang, S. Yang, *Organometallics* **2015**, *34*, 73−77.

[13] P. Štarha, A. Habtemariam, R. Romero-Canelón, G. J. Clarkson, P. J.Sadler, *Inorg. Chem.* **2016**, *55*, 2324–2331.

[14] a) R. Hu, J. L. Maldonado, M. Rodriguez, C. Deng, C. K. Jim, J. W. Y. Lam, M. M. F. Yuen, G. Ramos-Ortiz, B. Z. Tang, *J. Mater. Chem.* **2012**, *22*, 232–240; b) M. Banerjee, S. J. Emond, S. V. Lindeman, R. Rathore, *J. org. chem.* **2007**, *72*, 8054–8061.

[15] M. J. Frisch, G. W. Trucks, H. B. Schlegel, G. E. Scuseria, M. A. Robb, J. R. Cheeseman, *et al.* Gaussian 09, revision D.01; Gaussian, Inc.: Wallingford, CT, **2013**.

[16] X. C. Liu, J. F. Liang, J. You, L. Ying, Y. Xiao, S. R. Wang, X. G. Li, *Dyes Pigments* **2016**, *131*, 41–48.

[17] Z. Liu, A. Habtemariam, A. M. Pizarro, S. A. Fletcher, A. Kisova, O. Vrana, L. Salassa, P. C. A. Bruijnincx, G, J. Clarkson, V. Brabec, P. J. Sadler, *J. Med. Chem.* **2011**, *54*, 3011–3026.

[18] a) Y. L. Han, X. C. Liu, Z. Z. Tian, X. X. Ge, J. J. Li, M. Gao, Y. R. Li, Y. Liu, Z. Liu, *Chem. Asian J.* **2018**, *13*, 3697–3705; b) H. L. Hao, X. C. Liu, X. X. Ge, Y. Zhao, X. Tian, T. Ren, Y. Wang, C. F. Chao, Z. Liu, *J. Inorg. Biochem.* **2019**, *192*, 52–61.

[19] Z. Liu, R. J. Deeth, J. S. Butler, A. Habtemariam, M. E. Newton, P. J.Sadler, *Angew. Chem., Int. Ed.* **2013**, *52*, 4194–4197.

[20] a) Z. Liu, I. Romero-Canelón, B. Qamar, J. M. Hearn, A. Habtemariam, N. P. E. Barry, A. M. Pizarro, G. J. Clarkson, P. J. Sadler, *Angew. Chem., Int. Ed.* 2014, 53, 3941–3946; b) S. Betanzos-Lara, Z. Liu, A.

Habtemariam, A. M. Pizarro, B. Qamar, P. J. Sadler, *Angew. Chem., Int. Ed.* **2012**, *51*, 3897–3900.

[21] Y. L. Yang, L. H. Guo, Z. Z. Tian, X. C. Liu, Y. T. Gong, H. M. Zheng, X. X. Ge, Z. Liu, *Chem. Asian J.* **2018**, *13*, 2923–2933.

[22] a) V. Thamilarasan, P. Karunakaran, N. Kavitha, C. Selvaraju, N.Sengottuvelan, *Polyhedron* **2016**, *118*, 12–24; b) B. P. Espósito, R. Najjar, *Coord. Chem. Rev.* **2002**, *232*, 137–149.

[23] T. Keleş, B. Barut, Z. Biyiklioglu, A.Özel, *Dyes Pigments* **2017**, *139*, 575–586.

[24] R. Esteghamat-Panah, H. Hadadzadeh, H. Farrokhpour, J. Simpson, A. Abdolmaleki, F.Abyar, *Eur. J. Med. Chem.* **2016**, *127*, 958–971.

[25] D. Li, M. Zhu, C. Xu, B.Ji, *Eur. J. Med. Chem.* **2011**, *46*, 588–599.

[26] Pacheco, M. Emilia, L. Bruzzone, *J. Lumin.* **2013**, *137*, 138–142.

[27] J. Zhu, L. Wu, Q. Zhang, X. Chen, X. Liu, *Spectrochim. Acta. A* **2012**, *95*, 252–257.

[28] J. Tang, F. Luan, X. Chen, *Bioorg. Med. Chem.* **2006**, *14*, 3210–3217.

[29] S. Tabassum, R. Singh, M. Zaki, M. Ahmad, *RSC Adv.* **2015**, *5*, 35843–35851.

[30] A. Karabatsiakis, C. Böck, J. Salinas-Manrique, S. Kolassa, E. Calzia, D. E. Dietrich, I.-T. Kolassa, *Transl. Psychiatry* **2014**, *4*, 397.

[31] a) A. Tsuboyama, H. Iwawaki, M. Furugori, T. Mukaide, J. Kamatani, S. Igawa, T. Moriyama, S. Miura, T. Takiguchi, S. Okada, M. Hoshino, K. Ueno, *J. Am. Chem. Soc.* **2003**, *125*, 12971–12979; b) C. F. Chang, Y. M. Cheng, Y. Chi, Y. C. Chiu, C. C. Lin, G. H. Lee, P.-T. Chou, C.-C. Chen C.-H. Chang, C.-C. Wu, *Angew. Chem., Int. Ed.* **2008**, *47*, 4542–4545; c) G. Zhou, W. Y. Wong, B. Yao, Z. Xie, L. Wang, *Angewandte. Chemie.* **2007**, *119*, 1167-1169; d) Q. Zhao, F. Li, C. Huang, *Chem.Soc. Rev.* **2010**, *39*, 3007–3030.

[32] R. Pettinari, F. Marchetti, A. Petrini, C. Pettinari, G. Lupidi, B. Fernández, A. R. Diéguez, I, M. Nabissl, *Inorg. Chim. Acta.* **2017**, *454*, 139–148.

[33] a) Y. Zheng, L. He, D. Y. Zhang, C. P. Tan, L.-N Ji, Z. W. Mao, *Dalton. Trans.* **2017**, *46*, 11395–11407; b) C. Jin, J. Liu, Y. Chen, R. Guan, C. Ouyang, Y. Zhu, L.-N. Ji, H. Chao, *Sci. Rep.* **2016**, *6*, 22039.

10.1002/cbic.201900268

WILEY-VCH

Entry for the Table of Contents (Please choose one layout)

Layout 1:

FULL PAPER

Tetraphenylethylene appended organometallic Ir^{III} complexes show potential antineoplastic activity towards A549 cells. Half-sandwich Ir^{III} complexes could lead to the accumulation of reactive oxygen species (ROS) and induce apoptosis. Additionally, cycloiridium^{III} complexes could target lysosome, lead to lysosomal damage, and eventually induce apoptosis.

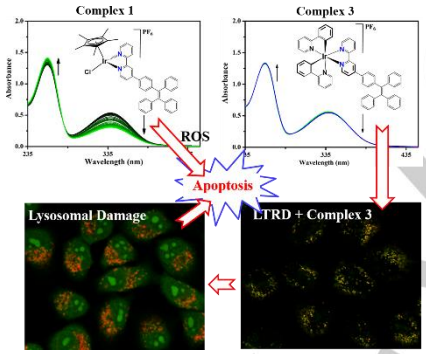

Xicheng Liu, Xiangdong He, Xiaojing Zhang, Yongling Wang, Jiaying Liu, Xiujuan Hao, Yue Zhang, Xiang-Ai Yuan, Laijin Tian, Zhe Liu**

Page No. – Page No.

Synthesis and Antineoplastic Applications of TPE Appended Organometallic Iridium(III) Complexes